

Persistence Bag-of-Words for Topological Data Analysis

Bartosz Zieliński, Michał Lipiński, Mateusz Juda
Jagiellonian University

{bartosz.zielinski,michal.lipinski,mateusz.juda}@uj.edu.pl

Matthias Zeppelzauer
St. Pölten University of Applied Sciences
m.zeppelzauer@fhstp.ac.at

Paweł Dłotko
Swansea University
p.t.dlotko@swansea.ac.uk

May 28, 2022

Abstract

Persistent homology (PH) is a rigorous mathematical theory that provides a robust descriptor of data in the form of persistence diagrams (PDs). PDs are compact 2D representations formed by multisets of points. Their variable size makes them, however, difficult to combine with typical machine learning workflows. In this paper, we introduce persistence bag-of-words, which is a novel, expressive and discriminative vectorized representation of PDs for topological data analysis. It represents PDs in a convenient way for machine learning and statistical analysis and has a number of favorable practical and theoretical properties like 1-Wasserstein stability. We evaluate our representation on several heterogeneous datasets and show its high discriminative power. Our approach achieves state-of-the-art performance and even beyond in much less time than alternative approaches. Thereby, it facilitates the topological analysis of large-scale data sets in future.

1 Introduction

Topological data analysis (TDA) provides a powerful framework for the structural analysis of high-dimensional data. An important tool in TDA is persistent homology, PH [15]. It provides a comprehensive, multiscale summary of the shape of the underlying data. PH is used to study qualitative properties of objects and currently gains increasing importance in data science [16]. It can

be efficiently computed using various currently available tools [4, 9, 10, 12, 14, 21]. A basic introduction to PH is given in Section 2 and a more detailed one in the supplementary material of this paper. The common output representation of PH are persistence diagrams (PDs) which are multisets of points in \mathbb{R}^2 . Due to their variable size, which depends on the characteristics of the input data, PDs are not easy to integrate within common data analysis, statistics and machine learning workflows. To alleviate this problem, a number of kernel functions and vectorization methods for PDs have been introduced.

Kernel-based approaches have a strong theoretical background but in practice they often become inefficient when the number of training samples is large. As the entire kernel matrix must usually be computed explicitly (like in case of SVMs), this leads to roughly quadratic complexity in computation time and memory with respect to the size of the input (training) set. Furthermore, such approaches are limited to kernelized methods, such as SVM and kernel PCA. Vectorized representations in contrast are compatible with a much wider range of methods and do not suffer from complexity constraints of kernels. They, however, often lack in representational power, as they require the spatial quantization of the PDs which is unusually non-adaptive and thus does not cope well with the sparseness of PDs.

In this work we present a novel adaptive and more precise representation of PDs which aims at combining the large representational power of kernel-based approaches

with the general applicability of vectorized representations. To this end, we extend the popular bag-of-words (BoW) encoding (originating from text and image retrieval) to TDA to cope with the inherent sparsity of PDs [22, 26]. The proposed adaptation of BoW gives a universally applicable fixed-sized feature vector of low-dimension. It is, under mild conditions, stable with respect to a standard metric in PDs and thus also theoretically builds upon a solid basis. Experiments demonstrate that our new representation achieves state-of-the-art performance and even outperforms numerous competitive methods while requiring orders of magnitude less time and being more compact.

The paper is structured as follows. Section 2 gives a basic introduction to PH and reviews related approaches. In Section 3 we introduce persistence bag-of-words and prove its stability. Sections 4 and 5 present the experimental setup and results. We conclude the paper in Section 6.

2 Background and Related Work

In this section, we first introduce persistence homology, an important tool in TDA, and then we describe state-of-the-art approaches, both kernel-based and vectorized, which make PH compatible with machine learning methods.

Under mild assumptions, persistent homology (PH) can be defined for a continuous function $f : X \rightarrow \mathbb{R}$, where $X \subset \mathbb{R}^n$. Typically f is a distance function from a collection of points, or a scalar value function defined on a grid of points, but in principle it can be an arbitrary function that satisfies a tameness assumption specified below. Focusing on sub-level sets $L_x = f^{-1}((-\infty, x])$, we let x grow from $-\infty$ to $+\infty$. While this happens, we can observe a whole hierarchy of events. In dimension zero, connected components of L_x will be created and merged together. One dimensional cycles that are not bounded, or higher dimensional voids will appear in L_x at critical points of f . The value of x on which a connected component, cycle or a higher dimensional void appears is refereed to as *birth time*. They will subsequently either became identical (up to a deformation) with other cycles and voids (created earlier), or they glue-in and become trivial. The value of x on which that happens is refereed to as *death*

time. Every connected component or cycle of a higher dimensional void can be annotated with a pair of its birth and death time, $[b, d]$. The length of the birth-death interval $[b, d]$ is often an indication whether the holes are structurally relevant or more likely noise. This observation can be summarized with one of many *stability theorems* for persistence [15] which state that a small change in the space X , or a function f implies a small change in the resulting collection of persistence intervals. It makes the PDs a robust tool in data analysis. PDs for three different input point clouds are shown in Fig. 1.

In this paper we will use an equivalent notation of PD with a birth-persistence pair $[b, p]$, where b is its birth, and $p = d - b$, called *persistence value*, is the difference between death and birth time of the considered feature. In addition, we assume that a given function f is *tame*, i.e. it induces a finite number of those birth-persistence points. The multi-set of the birth-persistence points is considered a *persistence diagram* (PD).

There are various metrics on PDs. To define them, the finite diagrams have to be enriched with an infinite collection of points $(b, 0)$, which are often referred to as “points in the diagonal” in standard persistence. They represent features that are born and immediately die. Having B and B' , enriched PDs, and considering all possible matchings $\eta : B \rightarrow B'$, 1-Wasserstein distance is defined as:

$$W_1(B, B') = \inf_{\eta: B \rightarrow B'} \sum \|x - \eta(x)\|_\infty$$

In the following, when considering stability of the representations, we will consider the stability with respect to 1-Wasserstein distance. A more in-depth introduction to PH is provided in Section 2 of the supplementary material.

Different approaches have been introduced to make PDs compatible with statistical analysis and machine learning methods, i.e. kernel-based approaches and vectorized representations. The goal of **kernel-based approaches** on PDs is to define dissimilarity measures (also known as kernel functions) to compare PDs and thereby make them compatible with kernel-based machine learning methods, such as support vector machines (SVMs) and kernel Principal Component Analysis (kPCA). Li et al. [20] combine the traditional bag-of-features (BoF) approach with PDs. Therefore, they use various distance functions between 0-dimensional PDs (bottleneck and

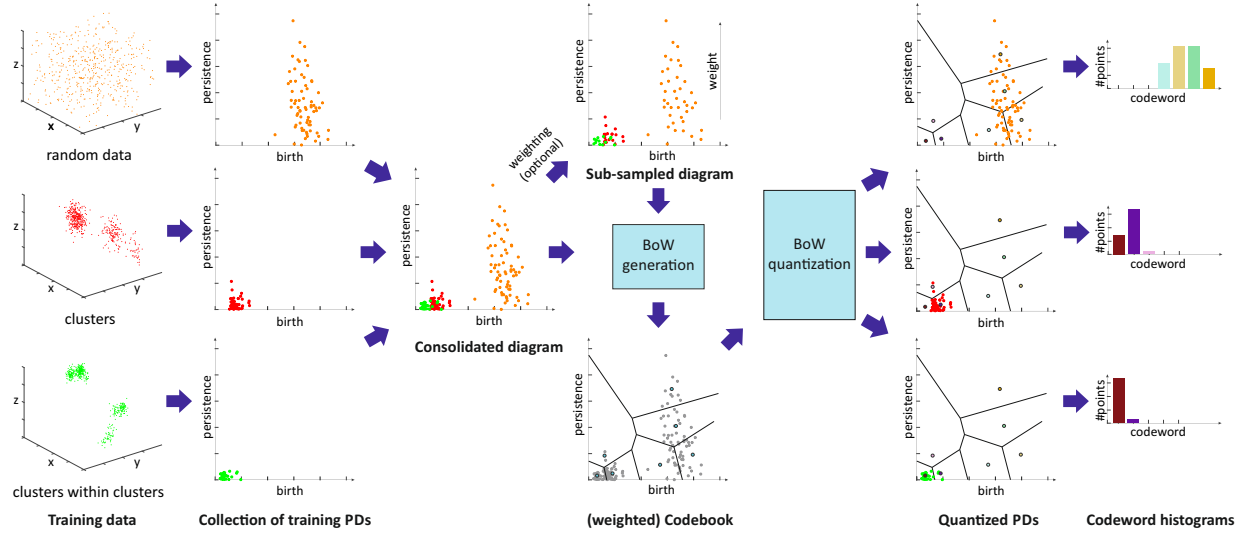


Figure 1: Persistence bag-of-words: An illustration of the entire pipeline for codebook generation and the extraction of codeword histograms. From the input data we compute PDs in birth-persistence coordinates and combine them into one consolidated diagram. Next, a subset of points is obtained from this diagram by either a weighted or unweighted sub-sampling. Subsequently, we cluster the sub-sampled consolidated diagram to derive a codebook. Finally, the individual points for each input PD are encoded by the codewords (BoW quantization). In this illustration a hard assignment of points to words is performed. The result is a codeword histogram for each input PD that represents how many points fall into which cluster of the codebook, i.e. codeword cardinalities. These codeword histograms represent a compact and fixed-size vectorial representation. It is worth mentioning that while the hard assignment presented here gives the idea of the procedure, often in practice we will use stable soft assignment.

Wasserstein distances for PDs, L^p distance functions for persistence landscapes of PDs) to generate kernels. On different datasets (SHREC 2010, TOSCA, hand gestures, Outex) they show that topological information is complementary to the information of traditional BoF.

Reininghaus et al. [25] proposed a kernel for persistence diagrams by turning PDs into a continuous distribution by appropriate placing of Gaussian distributions in \mathbb{R}^2 . Subsequently, they define a kernel as a scalar product of the two corresponding distributions. They apply topological descriptors together with the novel kernel to shape retrieval and texture classification. Carrière et al. [7] propose another kernel based on sliced Wasserstein approximation of the Wasserstein distance. The authors show that the kernel is not only stable, but also mimics bottleneck distances between PDs. They subsequently develop an approximation technique to reduce the kernel compu-

tation time. They apply it to 3D shape segmentation, texture classification, and orbit recognition in dynamical systems. Another approach for the representation of PDs are Persistence Landscapes, PL [6]. PL is a stable functional representation of a PD obtained from transforming it into a sequence of real-valued piece-wise linear functions. To compare two landscapes, the authors use standard L^p distance. This distance can be used to define a kernel function. Note that PL can also be transformed into a fixed-length vectorized representation by sampling the values of the landscape function. The authors however are not reporting of the use of vectorized PLs, therefore we will focus on the kernel derived from PLs.

Approaches for **vectorized representations** derive fixed-sized variants of the PD that can directly be used as input to current machine learning methods. One approach is the persistence image (PI) proposed by Adams

et al. [1]. It’s a vectorized representation of PD which is built upon earlier work on size functions [13, 17]. The PI can be employed directly as a feature vector in conventional machine learning techniques. PI lives in Euclidean space, which makes it easy to combine with other (non-topological) descriptors. Anirudh et al. [2] propose an approach based on Riemannian manifold (RM). Their method first transforms a PD into a Gaussian kernel which is a Riemannian manifold with Fisher-Rao metric. Next, they transform the manifold to a vector space and use PCA to reduce its dimension to a fixed size which allows to use SVM more effectively.

Recently, a third type of approach has been introduced, which tries to learn which points in the PD are of particular importance for the given task in a supervised manner [18]. This approach has promising properties, however, can only be used in cases where supervisory information (labels) is available during the construction of the representation. In our work we focus on representations that can be build independently from label information.

3 Persistence Bag of Words

In this section, we adopt the bag-of-words (BoW) model [22, 26] introduced in text and image retrieval for the quantization of PDs to a fixed length vectorial representation. The idea behind BoW is to quantize variable length input data into a fixed-size representation by a so called *codebook*. The codebook is generated from the input data in an unsupervised manner by using clustering. The basic assumption behind BoW is that the clusters (i.e. codewords) capture the intrinsic structure of the data and thereby represent an efficient vocabulary for the quantization of the data. Given a codebook C , every input point P (in a potentially high-dimensional space) is encoded by assigning points from P to the nearest codeword from C . In traditional BoW this encoding leads to a codeword histogram, i.e. a histogram for which each codeword from C counts how many points from P are closest to this codeword.

For the employed BoW approaches, three important hyperparameters need to be identified: (1) the clustering algorithm used to generate the codebook, (2) the size of the codebook, i.e., the number of clusters, and (3) the type of proximity encoding which is used to obtain the final de-

scriptors, i.e. hard and soft assignment. In this paper we use k-means and Gaussian Mixture Models (GMM) for clustering and the size of each codebook is optimized to maximize performance. In the following sections, we will describe two ways of generating codeword histograms based on the proximity of points from P to codewords in C .

The overall approach is visualized in Fig. 1. The input consists of a set of PDs extracted from all instances of a given dataset. First, all PDs are merged into one diagram. This consolidated diagram may then be sub-sampled to reduce the influence of noise. Based on the (sub-sampled) consolidated diagram, the codebook C is generated using clustering. For a given codebook we generate codeword histograms by different quantization strategies. Details of this procedure are provided in the following sections.

Before moving to the formulation of our approach, let us consider a direct adaptation of BoW [3, 26] to PDs. Given a collection of persistence diagrams D_1, D_2, \dots, D_n , we consolidate them into $D = D_1 \cup D_2 \cup \dots \cup D_n$ and obtain a codebook by using k -means clustering on D . Let $\{\mu_i \in \mathbb{R}^2, i = 1, \dots, N\}$ denote the centers of obtained clusters. Given a new PD $B = \{x_t \in \mathbb{R}^2\}_{t=1}^T, NN(x_t) = i \mid d(x_t, \mu_i) \leq d(x_t, \mu_j) \text{ for all } j \in \{1, \dots, N\}$. We define a *persistence bag of words* (PBoW) as a vector:

$$\mathbf{v}^{\text{PBoW}}(B) = (v_i^{\text{PBoW}}(B))_{i=1, \dots, N},$$

where $v_i^{\text{PBoW}}(B) = \text{card}\{x_t \in B \mid NN(x_t) = i\}$. In other words, v_i^{PBoW} captures the number of points from B , which are closer to μ_i than to any other μ_j .

Subsequently, $\mathbf{v}^{\text{PBoW}}(B)$ is normalized by taking the square root of each component (preserving the initial sign) and dividing it by the norm of the whole vector. This is a standard normalization for BoW [24] and is used to reduce the influence of outliers.

This direct adaptation of BoW to PDs is, however, not 1-Wasserstein stable. To show this, let us assume that we have two clusters with centers $\mu_1 = (0, 0), \mu_2 = (1, 0) \in \mathbb{R}^2$, and PD B containing only one point $x_1 = (\frac{1}{2} + \epsilon, 0)$, for some small $\epsilon > 0$. Then, $\mathbf{v}^{\text{PBoW}}(B) = [0, 1]$, because x_1 is closer to μ_2 than μ_1 . However, a small perturbation in B , e.g. by -2ϵ , changes the assignment of x_1 from μ_2 to μ_1 . In this case $B' = \{(\frac{1}{2} - \epsilon, 0)\}$ and $\mathbf{v}^{\text{PBoW}}(B') = [1, 0]$. In order to be stable in 1-

Wasserstein sense, PBoW should fulfill the following condition:

$$2 = |\mathbf{v}^{\text{PBoW}}(B) - \mathbf{v}^{\text{PBoW}}(B')| < C|x_1 - y_1| < 2C\epsilon,$$

therefore $C > 1/\epsilon$. As $\epsilon > 0$ can be arbitrarily small, there does not exist a constant C that meets this condition. Therefore PBoW is not stable.

In the next section, we will adopt BoW to better fit the structure of PDs and deal with the instability problem by using soft rather than hard assignments of points to clusters.

3.1 Stable Persistence Bag of Words

In this section we present two important adaptations of BoW for PDs. Firstly, we enforce the codeword selection to be preferential to higher persistence points. Secondly, we adopt soft assignment of points to the clusters and prove that such an approach guarantees stability of the representation.

An important consequence of the stability theorem for PDs is that points with higher persistence are typically considered more important than points with lower persistence. Therefore, when selecting the centers of clusters μ_i in BoW among D , preference should be given to higher persistence points. To integrate this into codebook generation we perform the clustering on a subset of points obtained by a weighted sampling of D . For the sub-sampling we use a piece-wise linear weighting function $w_{a,b} : \mathbb{R} \rightarrow \mathbb{R}$. Given $a < b$:

$$w_{a,b}(t) = \begin{cases} 0 & \text{if } t < a \\ (t - a)/(b - a) & \text{if } a \leq t < b \\ b & \text{if } b \leq t \end{cases}$$

and use it to weight the second coordinate (persistence) of the points in the PD. In our experiments we set a and b to the persistence values corresponding to 0.05 and 0.95 quantiles of the persistence coordinate of the points in D . Consequently, persistence points having higher values for function w are more likely to be sampled. Note that the sub-sampling does not guarantee that the points of highest persistence will be selected as centers of clusters, but it makes the probability of such an event considerably larger.

To account for the instability of PBoW shown in the previous section, we propose *stable persistence bag of*

words (sPBoW), in which, similarly like in case of PBoW, we first consolidate PDs in the initial step of construction, and then generate a GMM based on the sub-sampled points (e.g. by expectation maximization [23]). Let the parameters of the fitted GMM be $\lambda = \{w_i, \mu_i, \Sigma_i, i = 1, \dots, N\}$, where w_i , μ_i and Σ_i denote the weight, mean vector and covariance matrix of Gaussian i and N denotes the number of Gaussians. Given a PD B its stable PBoW is defined as:

$$\mathbf{v}^{\text{sPBoW}}(B) = \left(v_i^{\text{sPBoW}} = w_i \sum_{x_t \in B} p_i(x_t | \lambda) \right)_{i=1, \dots, N},$$

where $w_i > 0$, $\sum_{i=1}^N w_i = 1$, and $p_i(x_t | \lambda)$ is the likelihood that observation x_t was generated by Gaussian i :

$$p_i(x_t | \lambda) = \frac{\exp\{-\frac{1}{2}(x_t - \mu_i)' \Sigma_i^{-1} (x_t - \mu_i)\}}{2\pi |\Sigma_i|^{\frac{1}{2}}}.$$

This representation is stable w.r.t. 1-Wasserstein distance (see Section 3.1.1). The intuition behind this approach is to assign each point to *all* codewords, but with weight inversely proportional to the distance to the codewords.

3.1.1 Stability of Stable Persistence Bag of Words

Theorem Let B and B' be persistence diagrams with a finite number of non-diagonal points. Stable persistence bag of words, sPBoW with N words is stable with respect to 1-Wasserstein distance between the diagrams, that is

$$\|\mathbf{v}^{\text{sPBoW}}(B) - \mathbf{v}^{\text{sPBoW}}(B')\|_{\infty} \leq C \cdot W_1(B, B'),$$

where C is a constant.

Proof. Let $\eta : B \rightarrow B'$ be the optimal matching in the definition of 1-Wasserstein distance. For a fixed $i \in \{1, \dots, N\}$ we have:

$$\begin{aligned} \|v_i^{\text{sPBoW}}(B) - v_i^{\text{sPBoW}}(B')\|_{\infty} &= \\ \left\| w_i \sum_{x \in B} (p_i(x | \lambda) - p_i(\eta(x) | \lambda)) \right\|_{\infty} &\leq \\ |w_i| \sum_{x \in B} \|(p_i(x | \lambda) - p_i(\eta(x) | \lambda))\|_{\infty} \end{aligned}$$

As $p_i : \mathbb{R}^2 \rightarrow \mathbb{R}$ are Lipschitz continuous with the Lipschitz constants L_i , we get

$$\begin{aligned} |w_i| \sum_{x \in B} \|(p_i(x|\lambda) - p_i(\eta(x)|\lambda))\|_\infty &\leq \\ |w_i| \sum_{x \in B} \|(L_i(x - \eta(x)))\|_\infty &= \\ |w_i| L_i \sum_{x \in B} \|x - \eta(x)\|_\infty &= |w_i| L_i W_1(B, B') \end{aligned}$$

□

A natural question arising from the proof of sPBoW stability is whether this stability further extends to p -Wasserstein distances. We would like to indicate that since sPBoW are additive (consider the definition of additivity from [25]), they are not stable for a p -Wasserstein distance for any $p > 1$ as indicated in Theorem 3 in [25].

4 Experimental Setup

To evaluate the proposed persistence BoW representations (PBoW and sPBoW), we compare them with a number of state-of-the-art approaches including kernel-based methods as well as vectorized PD representations. The evaluation is performed on classification tasks involving different datasets representing heterogeneous data including among others 3D shapes, textures, and social media graphs.

4.1 Datasets

For the proposed evaluation we incorporate datasets which cover a wide range of different retrieval problems. Firstly, to provide a proof-of-concept, we evaluate all the approaches on a set of synthetically generated shape classes from [1]. It consists of six shape classes represented by point clouds of the geometrical objects (see Fig. 2 of the supplementary material for example shapes) which should be differentiated by the derived representations.

Additionally, we evaluate the approaches on real-world datasets for geometry-informed material recognition (GeoMat) [11], classification of social network

graphs (reddit-5k, reddit-12k) [18], analysis of 3D surface texture (PetroSurf3D) [28], and 3D shape segmentation [7]. Where available, we have used pre-computed PDs available with datasets to foster reproducibility and comparability. As the computation times for some of the considered methods, especially for kernel-based approaches, do not scale well with the sizes of datasets, we have decided to randomly sub-sample some of the datasets. A detailed description of all datasets, the PD computation and the sub-sampling is provided in Section 3 of the supplementary materials.

4.2 Compared Approaches

We compare our bag-of-word approaches with both kernel-based techniques and vectorized representations. Kernel-based approaches include: 2-Wasserstein distance^a (2Wd) [19], the multi-scale kernel^b (MK) of [25], and sliced Wasserstein kernel^c (SWK) [7]. Furthermore, we employ the persistence landscape^{d,e} (PL) representation and generate a kernel matrix by the distance metric defined in [6]. Vectorized PD representations include: persistence image^f (PI) [1] and the Riemannian manifold approach^g (RM) [2].

4.3 Setup

For all training and test samples from the datasets in Section 4.1 we consider the PDs of dimension 1 as a common input (cycles) since they best express the internal structure in the data and yielded the most promising results in related works [1, 8]. In the considered datasets no infinite intervals of dimension 1 occur. In cases where infinite intervals are present, there are different ways to proceed: (1) ignoring them, (2) substituting infinity with some (large) number or (3) building separate representations for finite and infinite diagrams. In the general case we recommend to compute persistence bag-of-words for PDs of all available dimensions separately and to combine them during modeling.

^ahttps://bitbucket.org/grey_narn/hera

^b<https://github.com/rkwitt/persistence-learning>

^ccode obtained from Mathieu Carrière

^d<https://www.math.upenn.edu/~diotko/persistenceLandscape.html>

^e<https://github.com/queenBNE/Persistent-Landscape-Wrapper>

^f<https://github.com/CSU-TDA/PersistenceImages>

^g<https://github.com/rushilnirudh/pdsphere>

The classification pipeline is as follows: for the kernel-based approaches we take the PDs as input and compute the kernel matrices for the training and test samples. Next we train an SVM from the explicit kernel matrices and evaluate it on the test data. For the vectorized representations we compute the respective feature vectors from the PDs and feed them into a linear SVM for training. This procedure allows for directly comparing kernel-based approaches and vectorized representations.

For all datasets, we aim at solving a supervised classification task. For each of them we employ 80% of the samples as training data and the remaining samples for testing. The only exception is the PetroSurf3D dataset for which a 50% split between training and testing samples is employed due to its large size. To decrease the dependency on the training data, each experiment is repeated 25 times with random sample selections for the training and the test set. For each experiment we provide the average performance in terms of classification accuracy together with the standard deviation across all repetitions.

To find optimal parameters for each evaluated approach, we run a grid search over their respective hyperparameters. The hyperparameters and their evaluated values for each approach are listed in Table 1 of the supplementary material.

Our evaluation is partitioned into two sets of experiments. EXP-A uses all related approaches on a sub-sampled version of the datasets, while EXP-B operates only on the vectorized representations and uses larger datasets. The reason for this is that for the larger datasets in our study it is infeasible to compute the explicit kernel matrices for the kernel-based approaches due to memory limitations. To still enable a fair comparison of all approaches, we sub-sample the datasets in EXP-A to reduce their size, i.e. by randomly selecting 25 (GeoMat), 100 (reddit-5k), 50 (reddit-12k) and 260 (PetroSurf3D) samples for each class. In EXP-B we solely evaluate the vectorized representations on the datasets as described in Section 4.1.

Ultimately, we run a Wilcoxon signed-rank test on the results, to identify which results significantly differ from the best obtained result and which ones do not and can thus be considered equally good (with p-value of 0.01).

The entire code of all experiments is implemented in Matlab. For external approaches we use the publicly available implementations of the original authors. For

clustering and bag-of-words encoding we employ the VLFeat library [27]. Our code will be published on paper acceptance.

5 Results

Table 1 summarizes the results obtained in our experiments for EXP-A and EXP-B. For each combination of dataset and approach we provide the obtained classification accuracy (including the standard deviation) and the processing time needed to construct the representations (excluding the time for classification). Note that for the synthetic dataset and the 3D shape segmentation dataset, results of EXP-A and EXP-B are equal, as no sub-sampling was needed to perform EXP-A.

Overall, for 5 out of 6 experiments in EXP-A and 2 out of 4 experiments in EXP-B, PBoW or sPBoW achieve state-of-the-art performance or above. In case of the GeoMat dataset the state-of-the-art performance is even outperformed by a large margin (+13.5% in EXP-A and +13.4% in EXP-B). From EXP-A we further observe that vectorized representations (including the proposed ones) in most cases outperform kernel-based approaches. Only for the synthetic and PetroSurf3D datasets the sliced Wasserstein kernel (which is the best kernel-based approach in average) can compete with the vectorized representation (PI). Among the compared vectorized representations, PI in most cases outperforms RM and will thus serve as the primary approach for comparison with our approaches in subsequent sections. When comparing the stable vs. unstable variants of PBoW, we observe that PBoW in most cases outperforms its stable equivalent. This is further studied in Section 5.1.

Large differences exist in the processing times of the different approaches. The highest runtimes are obtained for the kernel-based approaches going up to 32360.0 seconds for the PetroSurf3D dataset. The slowest kernel is 2Wd followed by MK, SWK and PL which are approximately one order of magnitude faster. For the vectorized approaches, PI takes longest to compute. The runtimes, however, vary strongly, depending on the resolution of the employed PI (note that we have estimated the optimal parameters for each dataset by a grid search over all hyperparameters, see Table 1 of the supplementary material). The RM representation is one to two magnitudes faster

| EXP-A | | | | | | | | | | | | |
|--------|-------------------|-------------|-------------------|-------------|-------------------|-------------|-------------------|-------------|-------------------|-------------|-------------------|-------------|
| Descr. | Synthetic | | GeoMat | | Reddit-5k | | Reddit-12k | | PetroSurf3D | | 3D Shape Segm. | |
| | Score | Time (sec.) | Score | Time (sec.) | Score | Time (sec.) | Score | Time (sec.) | Score | Time (sec.) | Score | Time (sec.) |
| 2Wd | 96.4 ± 2.6 | 162.0 | 38.3 ± 5.0 | 8128.0 | 41.8 ± 3.4 | 8064.0 | 34.0 ± 3.5 | 13952.0 | 73.7 ± 4.4 | 32360.0 | 64.5 ± 1.5 | 5792.0 |
| MK | 89.9 ± 2.9 | 37.5 | 17.9 ± 3.3 | 7251.0 | 38.7 ± 4.0 | 4071.0 | 34.1 ± 4.6 | 10004.0 | 78.4 ± 3.2 | 27821.6 | 71.6 ± 1.1 | 808.0 |
| SWK | 97.4 ± 1.7 | 23.9 | 49.8 ± 3.2 | 1927.0 | 47.0 ± 3.5 | 386.0 | 38.1 ± 4.2 | 1985.0 | 79.0 ± 4.9 | 3827.0 | 95.0 ± 0.7 | 2109.0 |
| PL | 95.0 ± 2.5 | 46.7 | 29.7 ± 4.7 | 1539.0 | 36.1 ± 4.0 | 1135.0 | 29.6 ± 4.2 | 1079.0 | 77.5 ± 3.4 | 3198.9 | 93.9 ± 0.5 | 2659.0 |
| PI | 97.2 ± 1.9 | 0.6 | 46.0 ± 3.4 | 3360.0 | 52.3 ± 3.6 | 1984.0 | 41.4 ± 3.8 | 2592.0 | 80.2 ± 3.1 | 307.5 | 95.5 ± 0.6 | 78.6 |
| RM | 91.8 ± 2.8 | 2.8 | 28.9 ± 2.6 | 12.7 | 51.4 ± 3.8 | 9.2 | 42.5 ± 4.5 | 45.7 | 79.6 ± 3.5 | 77.1 | 87.0 ± 0.8 | 4.1 |
| PBoW | 94.2 ± 2.4 | 0.5 | 63.3 ± 3.5 | 8.8 | 50.0 ± 3.4 | 2.9 | 40.5 ± 3.7 | 2.6 | 79.2 ± 2.7 | 2.4 | 92.0 ± 0.8 | 1.5 |
| sPBoW | 95.3 ± 2.2 | 2.4 | 52.8 ± 4.8 | 4.7 | 52.8 ± 3.2 | 0.9 | 40.0 ± 3.8 | 1.4 | 78.1 ± 4.0 | 2.9 | 95.2 ± 0.6 | 7.1 |

| EXP-B | | | | | | | | | | | | |
|--------|---------------|-------------|-------------------|-------------|-------------------|-------------|-------------------|-------------|-------------------|-------------|----------------|-------------|
| Descr. | Synthetic | | GeoMat | | Reddit-5k | | Reddit-12k | | PetroSurf3D | | 3D Shape Segm. | |
| | Score | Time (sec.) | Score | Time (sec.) | Score | Time (sec.) | Score | Time (sec.) | Score | Time (sec.) | Score | Time (sec.) |
| PI | same as EXP-A | | 33.5 ± 1.5 | 4960.0 | 49.8 ± 1.3 | 5280.0 | 43.1 ± 1.2 | 2272.0 | 79.1 ± 0.3 | 4608.0 | same as EXP-A | |
| RM | | | 11.4 ± 1.1 | 60.9 | 46.3 ± 1.2 | 112.0 | 38.0 ± 1.2 | 104.9 | 77.5 ± 0.5 | 591.0 | | |
| PBoW | | | 46.9 ± 1.4 | 8.9 | 48.9 ± 1.4 | 9.1 | 39.2 ± 1.3 | 9.0 | 78.7 ± 0.5 | 54.1 | | |
| sPBoW | | | 41.0 ± 1.5 | 28.5 | 44.8 ± 1.0 | 13.4 | 32.9 ± 1.4 | 21.8 | 78.1 ± 0.3 | 72.6 | | |
| | | | | | | | | | | | | |

Table 1: Results of EXP-A and EXP-B averaged over 25 runs. For each run we provide classification accuracy, its standard deviation and the computation time. Scores are computed as defined for the individual datasets. Results with statistically significant improved performance are highlighted bold. The first four approaches are kernels (2Wd: 2-Wasserstein Distance, MK: Multiscale Kernel, SWK: Sliced Wasserstein Kernel, PL: Persistence Landscape). The remaining approaches are vectorized representations evaluated in EXP-A and EXP-B (PI: Persistence image, RM - Riemmanian manifold, (s)PBoW: (stable) Persistence Bag-of-Words).

than PI^h . The proposed approaches outperform almost all state of the art approaches in runtime for all datasets, both for EXP-A and EXP-B. The gain in runtime efficiency ranges from one to up to four orders of magnitude. For the largest dataset in the experiments (PetrSurf3D), for example, the PBoW and sPBoW require 54.1 and 72.6 seconds while RM requires 591 seconds and PI 4608 seconds. In the following, we analyze selected aspects of the proposed representations in greater detail, such as runtime, scalability and sensitivity to parameters.

5.1 Accuracy vs. Codebook Size

The most important parameter for bag-of-words representations is the codebook size N , i.e. the number of clusters. There is no commonly agreed analytic method to estimate the optimal codebook size, thus the estimation is usually performed empirically. To investigate the sensitivity of (s)PBoW and their performance on the codebook size, we evaluate both approaches for N equals from 10 to 100 in steps of 10 for different datasets. The results are presented in Fig. 2, both without (solid lines) and with weighted sub-sampling (dashed lines) of the consolidated PD.

^hNote that for both representations we use the implementations provided by the original authors

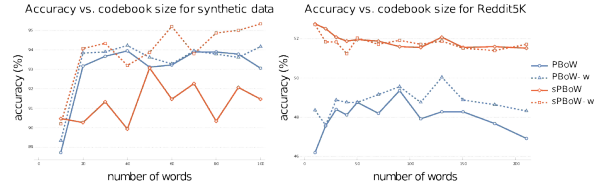


Figure 2: Accuracy vs. codebook size for datasets from EXP-A without (solid lines) and with codebook weighting (dashed lines). See plots for remaining datasets in Fig. 3 of the suppl. material.

On the synthetic dataset we observe that without weighting PBoW outperforms sPBoW. However, when codebook weighting is introduced, the stable variant sPBoW starts to outperform PBoW with larger codebook sizes. The trend shows that larger codebook sizes are better than small ones but also that with already 20 words a high performance can already be achieved. Using weighting and the stable formulation of PBoW clearly improves the performance on this dataset. In case of the social network graphs (reddit-5k), stability is extremely important, both in case of weighted and not weighted codebooks. At the same time, weighting has no influence on classification accuracy. Overall, we observe that the benefit of

weighting is dataset dependent and that no general recommendation can be derived for weighting (see also the results for the remaining datasets in Fig. 3 of the supplementary material). For three of the employed datasets (synthetic, reddit-5k, and 3D shapes) the stable formulation of PBoW outperforms the unstable one, for one dataset they perform almost equal (reddit-12k) and for two datasets (GeoMat and PetroSurf3D) the unstable variant is better. This is interesting as both datasets contain depth maps of surface textures. A closer investigation of this coincidence is subject of future work.

5.2 Time vs. Dataset Size

To investigate the runtime behavior of the proposed approaches in more detail, we evaluate how they scale for a varying number of input PDs, i.e. dataset size. To this end, we adapt the largest dataset (PetroSurf3D) and randomly sample different numbers of PDs, i.e. from 1000 to 10000 in steps of 1000. To get a detailed breakdown of computation time we measure the time needed for codebook generation, histogram assignment, and classification, separately. The computation of the PDs is not included in this breakdown. From the results presented in Fig. 3, we conclude that runtime grows linearly with the number of PDs. Most time is spent on codebook generation, where all PDs have to be consolidated and clustering is applied. Histogram assignment is faster in case of PBoW, because it is based on k-d trees [5], while in case of sPBoW, Gaussian likelihood has to be computed. One can also observe that SVM converge faster in case of the stable representation. The computational overhead of the sPBoW is in most cases small and grows only slowly with dataset size.

5.3 Qualitative Analysis

In this section we investigate our proposed with a special focus on their discriminative abilities. We employ the synthetic dataset for proof-of-concept and GeoMat for which we outperform other representation by a large margin.

We compute PBoW with $N = 20$ clusters for the **synthetic dataset** and visually analyze the codeword histograms obtained by (hard) assignment. For each of the six shape classes we compute the average codebook histogram (over all samples of each class) to ob-

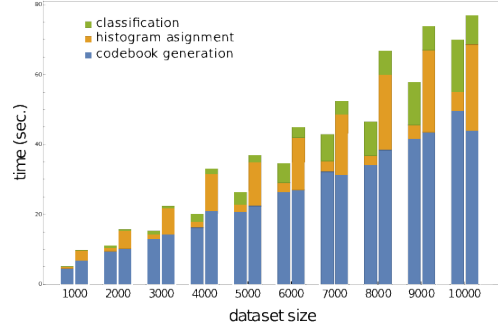


Figure 3: Time vs. dataset size for PBoW and sPBoW (left and right bar of each pair), both with $N = 50$. We measure the time needed for codebook generation (blue, bottom), histogram assignment (orange, middle), and classification (green, top), separately.

tain one representative PBoW vector per class. The averaged PBoW histograms for each classes are presented in Fig. 4. Instead of only providing the histograms themselves, we plot for each codeword of the histogram the corresponding cluster center as a circle in the original birth-persistence domain and encode the number of assigned codewords (the actual values of the histograms) in the area of the circles, i.e. the larger the count for a cluster, the larger the circle. The advantage of this representation is that the spatial distribution of the codewords in the PD is preserved.

From Fig. 4 we can see that except for the classes “random cloud” and “sphere” (which are difficult to differentiate) all classes generate strongly different cluster distributions. Class “circle”, for example, uniquely activates four clusters with strong persistence (top-left corner) and the “torus” class distributes its corresponding code words across a large number of clusters representing less persistent components.

Fig. 4 further illustrates an important property of persistence bag-of-words, namely its sparse nature. More specifically, areas with no points in the consolidated persistence diagram will contain no codewords (clusters). In Fig. 4, for example, no codeword is obtained in the upper-right quadrant of the diagram, since no components are located there for the underlying data. Thus these unimportant areas are neglected and not encoded into the final representation. This not only reduces the dimension of the

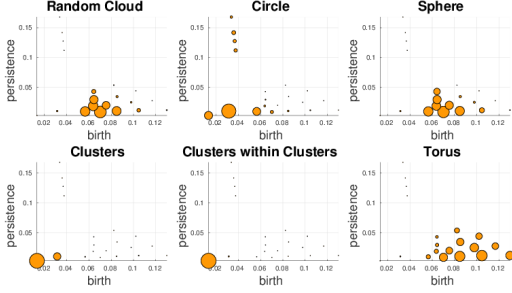


Figure 4: Average codebook histograms computed for each of the six shape classes of the synthetic dataset. The cluster center of each codeword is presented as a circle in the birth-persistence domain. The area of the circles reflects the histogram values of the specific class. For all classes the same codebook (same clustering) is employed, thus, dot locations are the same on all plots. Class differences are thus reflected by different sizes of the circles.

final representation but further makes the representation adaptive to the underlying data. Thereby the information density in the obtained representation increases.

We further investigate the performance on the **GeoMat** dataset to explain why (s)PBoW outperform all other representations by a large margin (see Table 1), first and foremost PI, which is the best related approach on this dataset in EXP-B. To this end, we generate confusion matrices for PI and PBoW (see Fig. 5 of the supplementary material) to determine pairs of classes where PBoW outperforms PI in discrimination.

Average PBoW histograms for two example classes (“cement smooth” and “concrete cast-in-place”) are shown in Fig. 5. For both classes the histograms are on the first sight similar (upper row in Fig. 5). However, by zooming-in towards the birth-persistence plane in Fig. 5 (bottom row), differences become better visible. The plots in the center illustrate the difference between the class distributions (red color means left class is stronger, blue means right class is stronger for this cluster). The classes differ by fine-grained spatial differences. The set of three blue points around birth time of 0 (which are characteristic for class “concrete cast-in-place”) surrounded by red points (which are characteristic for class “cement

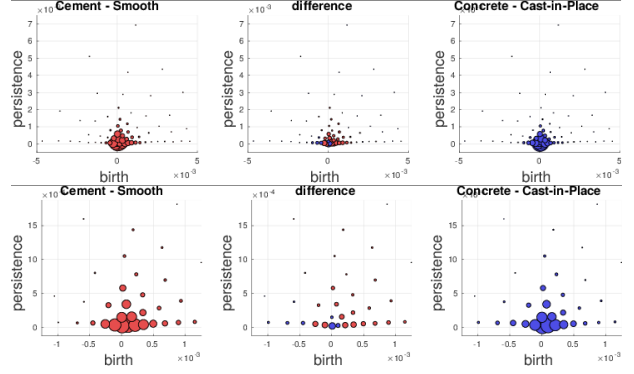


Figure 5: Comparison of averaged PBoW histograms for class “cement smooth” (left, red) and “concrete cast-in-place” (right, blue) from GeoMat (top row: total view, bottom row is zoomed in). The plot in the center shows the difference between the classes where red color means that the left class has stronger support for this cluster and blue means that the right class has stronger support.

smooth”) illustrates this well (see lower central plot). For the discrimination of these two classes a particularly fine-grained codebook with many clusters is needed. The PI has problems with such fine-grained structures, because due to its limited resolution, all topological components in the most discriminative area would most likely fall into one pixel. Therefore, an extraordinary high resolution would be necessary to capture the discriminative patterns between those two classes. The bag-of-words model makes our approaches independent of the resolution and enables to capture even fine differences adaptively. More examples from the GeoMat dataset can be found in Fig. 6 of the supplementary material.

6 Conclusion

We have introduced persistence bag-of-words, a novel vectorial representation for persistence diagrams that leverages the bag-of-words model. The novel representation has attractive theoretic properties, i.e. stability with respect to 1-Wasserstein distance as well as practical properties, i.e compactness, expressiveness, and adaptivity to sparseness. Experiments on six heterogeneous

datasets show that the novel representations achieve state-of-the-art and partly even better performance while requiring significantly less computation time. The high computational efficiency could in future facilitate the application of TDA to larger datasets than possible today.

Acknowledgements

The work from this article was supported by the National Science Centre, Poland under grant agreement no 2015/19/D/ST6/01215, by the Austrian Research Promotion Agency (FFG) under project no. 856333, and by EP-SRC grant “New Approaches to DataScience: Application Driven Topological Data Analysis” EP/R018472/1.

References

- [1] H. Adams, T. Emerson, M. Kirby, R. Neville, C. Peterson, P. Shipman, S. Chepushtanova, E. Hanson, F. Motta, and L. Ziegelmeier. Persistence images: a stable vector representation of persistent homology. *Journal of Machine Learning Research*, 18(8):1–35, 2017. 4, 6
- [2] R. Anirudh, V. Venkataraman, K. Natesan Ramamurthy, and P. Turaga. A riemannian framework for statistical analysis of topological persistence diagrams. In *Proceedings of the IEEE Conference on Computer Vision and Pattern Recognition Workshops*, pages 68–76, 2016. 4, 6
- [3] R. Baeza-Yates, B. Ribeiro-Neto, et al. *Modern information retrieval*, volume 463. ACM press New York, 1999. 4
- [4] U. Bauer, M. Kerber, J. Reininghaus, and H. Wagner. Phat—persistent homology algorithms toolbox. *Journal of Symbolic Computation*, 78:76–90, 2017. 1
- [5] J. L. Bentley. Multidimensional binary search trees used for associative searching. *Communications of the ACM*, 18(9):509–517, 1975. 9
- [6] P. Bubenik. Statistical topological data analysis using persistence landscapes. *Journal of Machine Learning Research*, 16(1):77–102, 2015. 3, 6
- [7] M. Carrière, M. Cuturi, and S. Oudot. Sliced wasserstein kernel for persistence diagrams. In *ICML*, 2017. 3, 6
- [8] M. Carrière, S. Oudot, and M. Ovsjanikov. Stable topological signatures for points on 3d shapes. In *Computer Graphics Forum*, volume 34, pages 1–12. Wiley Online Library, 2015. 6
- [9] C. Chen and M. Kerber. Persistent homology computation with a twist. In *Proceedings 27th European Workshop on Computational Geometry*, volume 11, 2011. 1
- [10] V. De Silva, D. Morozov, and M. Vejdemo-Johansson. Dualities in persistent (co) homology. *Inverse Problems*, 27(12):124003, 2011. 1
- [11] J. DeGol, M. Golparvar-Fard, and D. Hoiem. Geometry-informed material recognition. In *Proceedings of the IEEE Conference on Computer Vision and Pattern Recognition*, pages 1554–1562, 2016. 6
- [12] T. Dey, D. Shi, and Y. Wang. Simba: An efficient tool for approximating rips-filtration persistence via simplicial batch-collapse. In P. Sankowski and C. Zaroliagis, editors, *24th Annual European Symposium on Algorithms, ESA 2016, August 22-24, 2016, Aarhus, Denmark*, volume 57 of *LIPIcs*, pages 35:1–35:16. Schloss Dagstuhl - Leibniz-Zentrum fuer Informatik, 2016. 1
- [13] P. Donatini, P. Frosini, and A. Lovato. Size functions for signature recognition. In *Proc. SPIE*, volume 3454, pages 178–183, 1998. 4
- [14] H. Edelsbrunner and J. Harer. *Computational topology: an introduction*. American Mathematical Soc., 2010. 1
- [15] H. Edelsbrunner, D. Letscher, and A. Zomorodian. Topological persistence and simplification. *Discrete and Computational Geometry*, 28:511–533, 2002. 1, 2
- [16] M. Ferri. Persistent topology for natural data analysis — a survey. In A. Holzinger, R. Goebel, and V. Palade, editors, *Towards Integrative Machine Learning and Knowledge Extraction*, pages 117–133, Cham, 2017. Springer International Publishing. 1
- [17] M. Ferri, P. Frosini, A. Lovato, and C. Zambelli. Point selection: A new comparison scheme for size functions (with an application to monogram recognition). In *Computer Vision — ACCV’98: Third Asian Conference on Computer Vision Hong Kong, China, January 8–10, 1998 Proceedings, Volume I*, pages 329–337. Springer, 1998. 4
- [18] C. Hofer, R. Kwitt, M. Niethammer, and A. Uhl. Deep learning with topological signatures. In *Advances in Neural Information Processing Systems*, pages 1633–1643, 2017. 4, 6
- [19] M. Kerber, D. Morozov, and A. Nigmatov. Geometry helps to compare persistence diagrams. *Journal of Experimental Algorithmics (JEA)*, 22:1–4, 2017. 6
- [20] C. Li, M. Ovsjanikov, and F. Chazal. Persistence-based structural recognition. In *IEEE Conference on Computer Vision and Pattern Recognition (CVPR)*, pages 2003–2010. IEEE, 2014. 2
- [21] C. Maria, J.-D. Boissonnat, M. Glisse, and M. Yvinec. The gudhi library: Simplicial complexes and persistent homol-

- ogy. In *International Congress on Mathematical Software*, pages 167–174. Springer, 2014. 1
- [22] A. McCallum, K. Nigam, et al. A comparison of event models for naive bayes text classification. In *AAAI-98 workshop on learning for text categorization*, volume 752, pages 41–48, 1998. 2, 4
 - [23] N. M. Nasrabadi. Pattern recognition and machine learning. *Journal of electronic imaging*, 16(4):049901, 2007. 5
 - [24] F. Perronnin, J. Sánchez, and Y. Xerox. Large-scale image categorization with explicit data embedding. In *Computer Vision and Pattern Recognition (CVPR), 2010 IEEE Conference on*, pages 2297–2304. IEEE, 2010. 4
 - [25] J. Reininghaus, S. Huber, U. Bauer, and R. Kwitt. A stable multi-scale kernel for topological machine learning. In *2015 IEEE Conference on Computer Vision and Pattern Recognition (CVPR)*, pages 4741–4748, June 2015. 3, 6
 - [26] J. Sivic and A. Zisserman. Video google: A text retrieval approach to object matching in videos. In *Ninth IEEE International Conference on Computer Vision, 2003*, pages 1470–1477. IEEE, 2003. 2, 4
 - [27] A. Vedaldi and B. Fulkerson. VLFeat: An open and portable library of computer vision algorithms. <http://www.vlfeat.org/>, 2008. 7
 - [28] M. Zeppelzauer, B. Zieliński, M. Juda, and M. Seidl. A study on topological descriptors for the analysis of 3d surface texture. *Computer Vision and Image Understanding*, 2017. 6

Persistence Bag-of-Words for Topological Data Analysis Supplementary Materials

Bartosz Zieliński, Michał Lipiński, Mateusz Juda
Jagiellonian University

{bartosz.zielinski,michal.lipinski,mateusz.juda}@uj.edu.pl

Matthias Zeppelzauer
St. Pölten University of Applied Sciences
m.zeppelzauer@fhstp.ac.at

Paweł Dłotko
Swansea University
p.t.dlotko@swansea.ac.uk

May 28, 2022

1 Introduction

This document represents the supplementary material to the paper “Persistence Bag-of-Words for Topological Data Analysis”. Here we present additional background information as well as complementary information on the experimental setup and additional results of our analysis that could not be included in the paper due to spatial limitations.

2 Background on Persistent Homology

In this section we present basic introduction to persistent homology. Please consult [7, 8, 13] for more information.

Topological spaces are typically infinite objects and for the sake of data analysis they have to be finitely represented by simplified objects called *cell complexes*. Cell complexes are build from *cells*: topologically simple objects having the property that an intersection of every pair of cells is either empty, or yet another cell in the cell complex.

A *simplicial complex* is a particular instance of a general cell complex. It is a natural tool in the study of multi-dimensional point cloud data. Cells of simplicial complex are called *simplices* and, in this particular case, are

formed with convex hulls of collections of nearby points in the point cloud. Simplices are uniquely characterized by collection of points involved in their convex hulls. A simplicial complex \mathcal{X} need to satisfy the following property: for every pair of simplices $\sigma, \tau \in \mathcal{X}$, $\sigma \cap \tau$ is either empty or a simplex in \mathcal{X} .

Given a point cloud X with a distance or a similarity measure d and a parameter $r > 0$ one can define a *Vietoris-Rips complex* $VR(X, r)$. It is a simplicial complex whose every simplex $\sigma = \{v_0, v_1, \dots, v_k\}$ satisfy $d(v_i, v_j) \leq r$ for every $i, j \in \{0, \dots, k\}$. For every simplex $\sigma \in VR(X, r)$ one can define a diameter of σ being the largest distance between the points in σ . This gives a natural ordering of simplices in $VR(X, r)$: primarily by diameter of simplices and secondarily (when diameters of two simplices are the same) by inverse of the number of points in simplices^a. It is easy to see that every prefix of such a ordering forms a simplicial complex, and therefore any increasing sequence of numbers $0 < r_1 < r_2 < \dots < r_n$ yields a nested sequence of simplicial complexes:

$$\emptyset \subset X = VR(X, 0) \subset VR(X, r_1) \subset VR(X, r_2) \subset \dots \subset VR(X, r_n)$$

Another typical scenario when such a nested sequences

^aA number of points involved in the simplex minus one is a *dimension* of the simplex.

of cell complexes arises is the case of values of a function f discretized on a grid G . The function $f : G \rightarrow \mathbb{R}$ is typically an output of some numerical method. The grid G naturally corresponds to cubical complex \mathcal{G} , and the function f provides an ordering of maximal cubes in the complex. This ordering induce a nested sequence of cubical complex, very much like a nested sequence of Vietoris-Rips complexes discussed above.

To cover those and other possible cases later in this section we will focus on a general case of filtered cell complex:

$$\emptyset = \mathcal{C}_0 \subset \mathcal{C}_1 \subset \dots \subset \mathcal{C}_n = \mathcal{C}$$

keeping in mind that most typically it will coming from a point cloud, or numerical simulations on a grid.

Given each cell complex \mathcal{C}_i in the filtration one can define its homology, $H(\mathcal{C}_i)$. Rather than give a formal definition which can be found in [7], we will focus on the intuitive understanding of the concept. Homology in dimension 0 measures number of connected components. In dimension 1 it measures the cycles which do not bound a (deformed) surface. In dimension 2 it corresponds to voids, i.e. regions of space totally bounded by a collection of triangles (very much like a ball bounds the void inside it). The idea of a cycle bounding a hole in the complex can be formalized using homology theory for arbitrary dimension.

Persistent homology measures the evolution of homology for the constitutive complexes in a filtration. Once more and more cells are being added to a complex \mathcal{C}_i , new connected components or cycles may appear, old one may became trivial, or became identical (homologous) to others created earlier. For every connected component or a cycle, there are two important characteristics we will be storing: The first moment b , refereed as a *birth time*, when it appears in the filtration and the last moment d , referred to as *death time*, when it either became trivial, or became identical to other cycle that has been created earlier. Instead of a standard birth-death summaries of persistent homology in this paper we use birth-persistence coordinates, which can be obtained by the $[b, d] \rightarrow [b, d - b]$ transformation. It is useful to relate the abstract machinery of PH with geometric intuition. To do that let us concentrate on a Fig. 1. Over there, on the left, a collection of points sampled from a circle is presented. Moving to the right reveals various stages of construction of a Vietoris-

Rips complex for an increasing sequence of radii. Along with increasing radius, simplices of increasing diameters are added to the complex. The key observation is that we can see a cycle for all the stages of the construction except from the initial and the final one. PH will capture this observation by outputting a long persistence interval in dimension one (visualized in the picture), spreading from the radius corresponding to the second to the radius corresponding to the last stage of the construction. This simple example illustrates the basic geometrical idea behind PH.

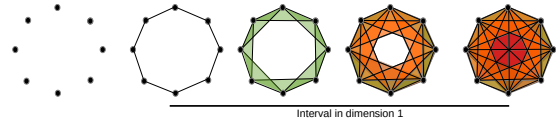


Figure 1: Various stages of construction of a Vietoris-Rips complex for eight points sampled from a circle. Initially, for sufficiently small radius, only vertices are present in the complex. Gradually more and more edges along with higher dimensional simplices of increasing diameter are added. In all but the initial and final stage of the construction the topology of a circle is visible, and therefore will be recovered by PH in dimension one (depicted by the long bar below the picture).

We have a couple of assumptions about PDs. Firstly, as our aim is to perform computations, we assume that persistence diagrams consist of finitely many points of nonzero persistence. Secondly, PDs may also contain infinite intervals that correspond to so called *essential classes*, i.e. the cycles that are born but never dies. Those infinite intervals needs to be processed prior to the computations. There are at least three strategies one can apply:

1. To ignore infinite intervals, and use only the finite ones in the consideration.
2. To substitute $+\infty$ in the death coordinates of the essential classes with a number N chosen by the user. A logical choice would be a number which is larger than a filtration value of any cell in the considered complex.
3. To build a pair of descriptors: one for finite, and one for infinite intervals and use them together as a final descriptor.

Given the available options in the numerical experiments presented in this paper we have chosen the simplest option, i.e. to ignore the infinite intervals. There are various classical metrics used to compare persistence diagrams [7]. We will review them here, as they are essential in the study of stability of the presented representations. Note that the presentation is a bit non standard, as we are working on birth-persistence coordinates. Given two diagrams B and B' , we construct a matching $\eta : B \rightarrow B'$ assuming that points can also be matched to $y = 0$ axis. Putting B and B' in the same diagram, one can visualize a matching η by drawing a line segment between $x \in B$ and $\eta(x)$ (note that $\eta(x)$ is either in B' , or is a projection of x to its first coordinate). Given all the line segments, for each matching we can store the longest one, or a sum of lengths of all of them (to a power q). Taking the minimum over all possible matchings of the obtained numbers will yield the *bottleneck* distance in the first case, and the *Wasserstein* distance (to the power $\frac{1}{q}$) in the second case. More formally:

Definition q -Wasserstein distance between two persistence diagrams $B, B' \in \mathcal{D}$ is defined as:

$$W_q(B, B') := \left[\inf_{\eta: B \rightarrow B'} \sum_{x \in B} \|x - \eta(x)\|_\infty^q \right]^{\frac{1}{q}}.$$

In particular:

$$W_1(B, B') := \inf_{\eta: B \rightarrow B'} \sum_{x \in B} \|x - \eta(x)\|_\infty.$$

An important feature of persistent homology is its *stability*. Intuitively, it indicates that small changes in the filtration implies small changes (for instance in Wasserstein metric) in the resulting persistence diagrams. Formally:

Theorem [7] Let X be a finite cell complex and $f, g : \mathbb{X} \rightarrow \mathbb{R}$ filtering Lipschitz functions. Let B and B' be the PDs of X with filtration induced by f and g respectively. Then there exist constants C and k such that $W_1(B, B') \leq C \|f - g\|_\infty^{1-k}$.

In this paper, we show stability of sPBoW with respect to 1-Wasserstein distance. Combined with the stability result from above, this indicates stability of sPBoW with respect to the perturbation of initial data.

3 Datasets

For our evaluation we incorporate a number of datasets which cover a wide range of different retrieval tasks. Firstly, to provide a proof-of-concept we evaluate all the approaches on a synthetically generated shape classes from [1]. Next, the approaches are evaluated on real-world datasets for geometry-informed material recognition (GeoMat) [5], classification of social network graphs (Reddit) [9], analysis of 3D surface texture (PetroSurf3D) [12], and 3D shape segmentation [2]. All the datasets are discussed in details in the following sections.

As the computation times for some of the considered methods, especially for kernel based approaches, do not scale well with the sizes of datasets, we have decided to sub-sample some of them (see Section 4.3 of the paper for details).

3.1 Synthetic Dataset

The first dataset we are going to consider is the synthetic dataset introduced by Adams et al. [1]. It consists of six shape classes represented by point clouds of the following geometrical objects: unit cube, circle of diameter one, sphere of diameter one, three clusters with centers randomly chosen from unit cube, hierarchical structure of three clusters within three clusters (where the centers of the minor clusters are chosen as small perturbations from the major cluster centers), and a torus (see Fig. 2 for example shapes). Each point cloud is perturbed by positioning a Gaussian distribution of standard deviation 0.1 at this point and sampling novel points from the distribution. Overall this dataset contains 50 point clouds for each of the six classes, each containing 500 3D points. This gives 300 point clouds in total.

From each point cloud we compute the PDs in dimension 1 for a Vietoris-Rips filtration for a radius parameter equal to the maximal distance between points in the point cloud. For this purpose, we employ the approximation method proposed by Dey et al. [6] and the SimBa implementation based on the work of Dayu Shi^b.

^b<http://web.cse.ohio-state.edu/~dey.8/SimBa/Simba.html>, last visited October, 2018

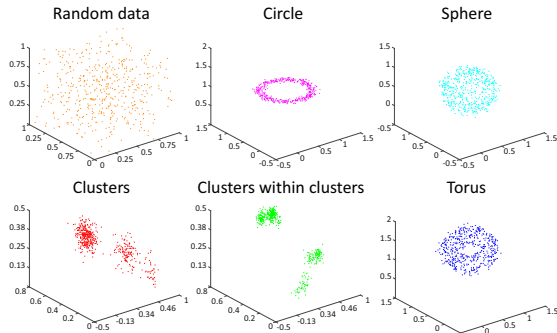


Figure 2: Example shapes from the six shape classes of the synthetic dataset.

3.2 Geometry-Informed Material Recognition Dataset (GeoMat)

The GeoMat dataset contains a collection of materials and provides geometry information (point clouds) as well as visual images of 19 different materials, such as “brick”, “grass” and “gravel” [5]. The GeoMat dataset contains patches sampled from larger photographs of surfaces from buildings and grounds. Each patch predominantly represents only one material. Each class consists of 600 images, each of size 100×100 pixels. Among them, there are pictures of different scales, i.e. 100×100 , 200×200 , 400×400 and 800×800 .

To keep dataset at a reasonable size for our experiments, we selected only patches of resolution 400×400 , which results in 149 patches for each of the 19 categories. For each patch, the dataset provides a depth image^c. The depth images contain the local (fine-grained) surface texture as well as the global surface curvature. To filter out the global curvature we transformed each depth image into a point cloud in 3D space, consisting of 10000 points (every point represents one of the 100×100 pixels). Next, point cloud were rotated in a way that the Z axis represents depth, then removed the global surface curvature by fitting a second degree function (paraboloid) to the point cloud, which values were finally subtracted from the Z coordinates of the points. The values of the Z-coordinates were then centered at 0. Finally, the point

cloud was projected back into a bitmap (depth map), with the Z-coordinates as depth values. Ultimately, we computed PDs by grayscale filtration.

3.3 Social Network Graphs Datasets (Reddit)

To evaluate our approaches on a broad range of possible input data, we further incorporate graph-based datasets in our evaluation. To this end we employ the reddit-5k and reddit-12k datasets from [11], which contain discussion graphs from the reddit platform^d. Nodes in the graphs correspond to users and edges between users exist if one user has commented a posting of the other user. Different graphs are labeled by subreddits, which refer to different topics. The dataset reddit-5k contains overall 5000 graphs for 5 popular subreddits. For the larger dataset reddit-12k we sample 5.643 graphs for 11 subreddits including topics like, e.g. “worldnews”, “videos” and “atheism”. The task for both datasets is to predict the subreddit (topic) from the input graph. For both datasets we use the pre-computed PDs from^e.

3.4 3D Surface Texture Dataset (PetroSurf3D)

A further dataset in our experiments is the recently released *PetroSurf3D* dataset, which contains high-resolution 3D surface reconstructions from the archaeological domain with a resolution of approximately 0.1mm [10]. The reconstructions represent 26 natural rock surfaces that exhibit human-made engravings (so-called rock art) and thereby exhibit complex 3D textures. The classification task for PetroSurf3D is to automatically predict which areas of the surface contain engravings and which not, i.e. there are two classes of surface topographies: engraved areas and the natural rock surface. Engraved areas represent approximately 19% of the data. For each surface a precise pixel-accurate ground truth exists together with a depth map of the surface. The depth maps are analyzed in a patch-wise manner. Overall, there are 754.386 patches to classify for all 26 surfaces. For our

^cSource: http://web.engr.illinois.edu/~degol2/pages/MatRec_CVPR16.html, last visited August 2018

^dReddit is a content-aggregation website: <http://reddit.com>
^eSource: <https://github.com/c-hofer/nips2017>, last visited October, 2018

experiments we randomly select 13 surfaces as a training set and employ the remaining ones for evaluation. The training set is further sub-sampled (to keep the number of training samples in a practical range). Overall, a balanced set (equal class cardinalities) of 600 patches per surface ($13 * 600 = 7800$ samples) is used for training. The testing set contains a balanced subset of 600 random samples from each of the remaining 13 surfaces. For each patch a PD is computed by grayscale filtration as a basis for our experiments.

3.5 3D Shape Segmentation Dataset

We further employ the 3D shape dataset from [4] which was preprocessed by Carrière et al. [3] for topological data analysis. The preprocessed dataset contains PDs for 5700 3D points from airplane models. Each point is assigned to one sub-part (segment) of an airplane, e.g., 'wing', 'vertical stabilizer' and 'horizontal stabilizer'. For our experiments we use the PDs computed by Carrière et al. [3] from their repository^f. The PDs were generated by tracking topology evolution of a geodesic ball centered at the individual points of the input 3D model. The radius thereby grows from 0 to infinity. We focus on PDs of dimension 1 as the considered 3D shapes are connected. The task is to classify each point according to the segment it belongs to. By classifying each point a segmentation of the airplane into its parts is finally obtained.

4 Evaluated Parameters

To find optimal parameters for each evaluated approach, we run a grid search over their respective hyperparameters. The hyperparameters and their evaluated values for each approach are listed in Table 1, both for EXP-A and EXP-B. The optimal parameters are highlighted in bold. For each parameter combination we run a complete experiment (25 iterations) to evaluate its performance.

^fSource: https://github.com/MathieuCarriere/sklearn_tda, last visited October 2018

| EXP-A | | | | | | |
|--------|-----------|--|---|---|--|---|
| Descr. | Synthetic | GeoMat | Reddit-5k | Reddit-12k | PetroSurf3D | 3D Shape Segm. |
| MK | σ | $\{0.5\}$ | $\{0.5\}$ | $\{0.5\}$ | $\{0.5\}$ | $\{0.5\}$ |
| SWK | n | $\{50, 100, 150, 200, 250\}$ | $\{50, 100, 150, 200, 250\}$ | $\{50, 100, 150, 200, 250\}$ | $\{50, 100, 150, 200, 250\}$ | $\{50, 100, 150, 200, 250\}$ |
| PI | r | $\{10, 20, 40, 60, 80, 100, 120, 140, 160, 180, 200\}$ | $\{10, 20, 30, 40, 60, 80, 100, 120, 140, 170, 200\}$ | $\{10, 20, 30, 40, 60, 80, 100, 120, 140, 170, 200\}$ | $\{5, 10, 20, 30, 40, 50, 60, 70, 80, 90, 100\}$ | $\{10, 20, 30, 40, 50, 60, 70, 80, 90, 100\}$ |
| | σ | $\{0.1, 0.25, 0.5, 0.75, 1, 1.5, 2\}$ | $\{0.1, 0.25, 0.5, 0.75, 1, 1.5, 2\}$ | $\{0.1, 0.25, 0.5, 0.75, 1, 1.5, 2\}$ | $\{0.1, 0.25, 0.5, 0.75, 1, 1.5, 2\}$ | $\{0.1, 0.25, 0.5, 0.75, 1, 1.5, 2\}$ |
| | W | $\{W, NW\}$ | $\{W, NW\}$ | $\{W, NW\}$ | $\{W, NW\}$ | $\{W, NW\}$ |
| RM | r | $\{5, 10, 20, 40\}$ | $\{5, 10, 20, 40, 60\}$ | $\{10, 20, 40, 60\}$ | $\{10, 20, 40, 60\}$ | $\{10, 20, 40\}$ |
| | σ | $\{0.1, 0.2, 0.3\}$ | $\{0.0001, 0.0005, 0.001, 0.005, 0.01, 0.05, 0.1\}$ | $\{0.0001, 0.0005, 0.001, 0.005, 0.01, 0.05, 0.1\}$ | $\{0.01, 0.05, 0.1, 0.2, 0.3\}$ | $\{0.01, 0.05, 0.1, 0.2, 0.3\}$ |
| | d | $\{25, 50, 75, 100\}$ | $\{25, 50, 75, 100\}$ | $\{25, 50, 75, 100\}$ | $\{25, 50, 75, 100\}$ | $\{25, 50, 75, 100\}$ |
| PBoW | N | $\{10, 20, 30, 40, 50, 60, 70, 80, 90, 100\}$ | $\{10, 20, 30, 40, 50, 70, 90, 110, 130, 150, 180, 210\}$ | $\{10, 20, 30, 40, 50, 70, 90, 110, 130, 150, 180, 210\}$ | $\{5, 10, 20, 30, 40, 50, 60, 70, 80, 90, 100\}$ | $\{10, 20, 30, 40, 50, 60, 70, 80, 90, 100, 120, 130, 140, 150\}$ |
| | W | $\{W, NW\}$ | $\{W, NW\}$ | $\{W, NW\}$ | $\{W, NW\}$ | $\{W, NW\}$ |
| sPBoW | N | $\{10, 20, 30, 40, 50, 60, 70, 80, 90, 100\}$ | $\{10, 20, 30, 40, 50, 70, 90, 110, 130, 150, 180, 210\}$ | $\{10, 20, 30, 40, 50, 70, 90, 110, 130, 150, 180, 210\}$ | $\{5, 10, 20, 30, 40, 50, 60, 70, 80, 90, 100\}$ | $\{10, 20, 30, 40, 50, 60, 70, 80, 90, 100, 120, 130, 140, 150\}$ |
| | W | $\{W, NW\}$ | $\{W, NW\}$ | $\{W, NW\}$ | $\{W, NW\}$ | $\{W, NW\}$ |
| EXP-B | | | | | | |
| Descr. | Synthetic | GeoMat | Reddit-5k | Reddit-12k | PetroSurf3D | 3D Shape Segm. |
| PI | r | $\{20, 50, 80, 110, 140\}$ | $\{10, 20, 30, 40, 60, 80, 100\}$ | $\{10, 20, 30, 40, 50, 60, 80, 100\}$ | $\{5, 10, 20, 30, 40, 50\}$ | same as EXP-A |
| | σ | $\{0.1, 0.25, 0.5, 0.75, 1, 1.5, 2\}$ | $\{0.1, 0.25, 0.5, 0.75, 1, 1.5, 2\}$ | $\{0.1, 0.25, 0.5, 0.75, 1, 1.5, 2\}$ | $\{0.1, 0.25, 0.5, 0.75, 1, 1.5, 2\}$ | same as EXP-A |
| | W | $\{W, NW\}$ | $\{W, NW\}$ | $\{W, NW\}$ | $\{W, NW\}$ | same as EXP-A |
| RM | r | $\{10, 20, 40, 60\}$ | $\{10, 20, 40, 60\}$ | $\{10, 20, 40, 60\}$ | $\{5, 10, 20, 40\}$ | same as EXP-A |
| | σ | $\{0.0001, 0.0005, 0.001, 0.005, 0.01, 0.05, 0.1\}$ | $\{0.0001, 0.0005, 0.001, 0.005, 0.01, 0.05, 0.1\}$ | $\{0.0001, 0.0005, 0.001, 0.005, 0.01, 0.05, 0.1\}$ | $\{0.05, 0.1, 0.2, 0.3\}$ | same as EXP-A |
| | d | $\{25, 50, 75, 100\}$ | $\{25, 50, 75, 100\}$ | $\{25, 50, 75, 100\}$ | $\{25, 50, 75, 100\}$ | same as EXP-A |
| PBoW | N | $\{20, 50, 80, 110, 140, 170, 200\}$ | $\{5, 10, 20, 30, 40, 50, 60, 80, 100, 120\}$ | $\{5, 10, 20, 30, 40, 50, 60, 80, 100, 120\}$ | $\{5, 10, 20, 30, 40, 50\}$ | same as EXP-A |
| | W | $\{W, NW\}$ | $\{W, NW\}$ | $\{W, NW\}$ | $\{W, NW\}$ | same as EXP-A |
| sPBoW | N | $\{20, 50, 80, 110, 140, 170, 200\}$ | $\{5, 10, 20, 30, 40, 50, 60, 80, 100, 120\}$ | $\{5, 10, 20, 30, 40, 50, 60, 80, 100, 120\}$ | $\{5, 10, 20, 30, 40, 50\}$ | same as EXP-A |
| | W | $\{W, NW\}$ | $\{W, NW\}$ | $\{W, NW\}$ | $\{W, NW\}$ | same as EXP-A |

Table 1: Parameters tested for EXP-A and EXP-B. The optimal parameters are highlighted in bold. Abbreviations: σ is scale parameter in MK, n is the number of lines slicing the plane in SWK, r is resolution of PI or density map in RM, σ is the sigma of the Gaussians employed, W is weighting (either no weighting (NW) or with weighting (W)), d is the dimension of principal geodesic analysis on the hypersphere, N is the number of codewords of persistence bag-of-words.

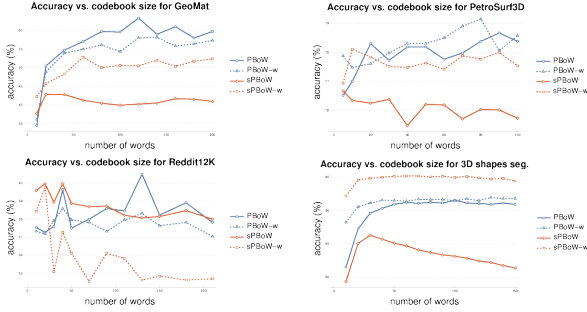


Figure 3: Accuracy vs. size of a codebook for datasets from EXP-A without (solid lines) and with codebook weighting (dashed lines).

5 Additional Results

In this section we provide additional investigations on selected aspects of the novel representations and provide additional illustrations and figures which were not included in paper due to spatial limitations.

5.1 Accuracy vs. Codebook Size

In Fig. 3 we present the sensitivity of the proposed approaches on the codebook size for the remaining datasets to complement Fig. 2 in Section 5.1 of the paper.

5.2 Accuracy vs. Time

Table 1 of the paper shows that our approaches achieve state-of-the-art or even better performance on almost all of the evaluated datasets. Furthermore they outperform all methods in speed. While the table shows only results for the optimal parameters (from the point of view of classification accuracy), here, we analyze the relation between accuracy and time in more detail. For this purpose, we use PI as a reference for comparison, as it represents the strongest competitor (in the sense of accuracy) of the proposed representations.

In Fig. 4, we plot accuracy vs. time for the proposed approaches and PI for four datasets from EXP-B. We decided to focus on EXP-B here, because it operates on the larger datasets. We vary the codebook size as well as the resolution of PI according to the values provided in Table 1 of the supplementary material. This directly influ-

ences the output dimension of the representation and is reflected by the area of the circles in Fig. 4, i.e. larger diameter means higher dimension. Note that experiments on PBoW were performed on 1 CPU while experiments on PI were performed in parallel on 32 CPUs. Thus the runtime differences are in fact even larger than depicted. For more compact visualization (and avoiding a logarithmic scale which would compress too much) we decided not to take the number of CPUs into account for plotting. We can see clearly that the runtime of PI is always significantly larger than for PBoW and sPBoW. The accuracy obtained varies. For all datasets except reddit-12k the performance level of PI is reached (or even superseded) much quicker. In the case of GeoMat dataset PBoW and sPBoW clearly outperform PI (while consuming much less time) and in case of PetroSurf3D and reddit-5k they quickly achieve a similar performance level. The computational cost of achieving a higher performance with PI e.g. in the case of reddit-12k is over-proportionally high while the performance gain is actually rather limited (approx. +1%).

5.3 Qualitative Analysis

In Fig. 5, we show the confusion matrix for PI and PBoW on the GeoMat dataset. The matrices show that PBoW achieves a higher number of correct classifications (see the higher values along the diagonal) and less class confusions (lower values for off-diagonal values). A detailed investigation on the discriminative abilities of PBoW between the classes “cement smooth” and “concrete cast-in-place” (i.e. classes 4 and 5) is presented in Fig. 5 of the paper. In Fig. 6 we show a similar comparison for classes “brick” and “concrete cast-in-place” (i.e. classes 2 and 5). Also in this example we can observe that spatially fine-grained differences distinguish the classes from each other. The adaptive nature of the bag-of-words model adapts well to such structures.

References

- [1] H. Adams, T. Emerson, M. Kirby, R. Neville, C. Peterson, P. Shipman, S. Chepushtanova, E. Hanson, F. Motta, and L. Ziegelmeier. Persistence images: a stable vector representation of persistent homology. *Journal of Machine Learning Research*, 18(8):1–35, 2017. 3

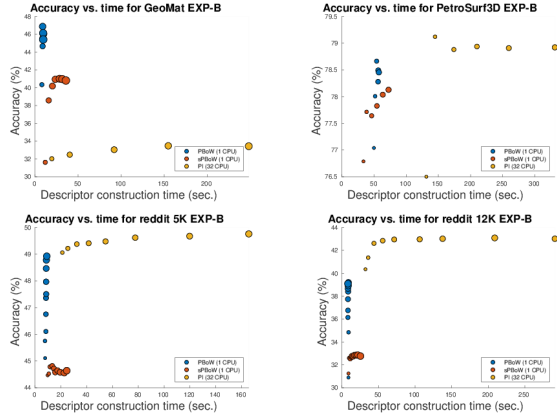


Figure 4: Accuracy vs. time for PBoW and sPBoW compared with PI (the strongest related representation) applied to four datasets from EXP-B. The size of colored points represents the size N of codebooks or the resolution r of PI (evaluated values for N and r are those listed in Table 1 of the supplementary material). Note that, the actual time of computation for the construction of the representations are presented. Codebooks were computed on 1 CPU while PI was constructed by using 32 CPUs in parallel. Moreover, SVM training and prediction time was not taken into consideration. This would further increase computational times especially for PI due to their larger dimension.

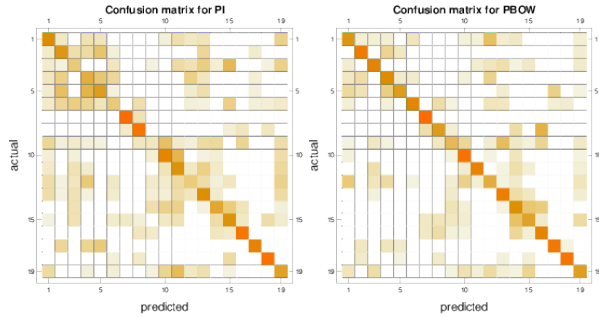


Figure 5: Confusion matrix for PI (left) and PBoW (right) on the GeoMat dataset from EXP-A. From the diagonal of the matrices we can see that PBoW outperforms PI for many classes (e.g. classes 2-5, 9 and 12. Furthermore, there are less confusions (off-diagonal values) for PBoW.

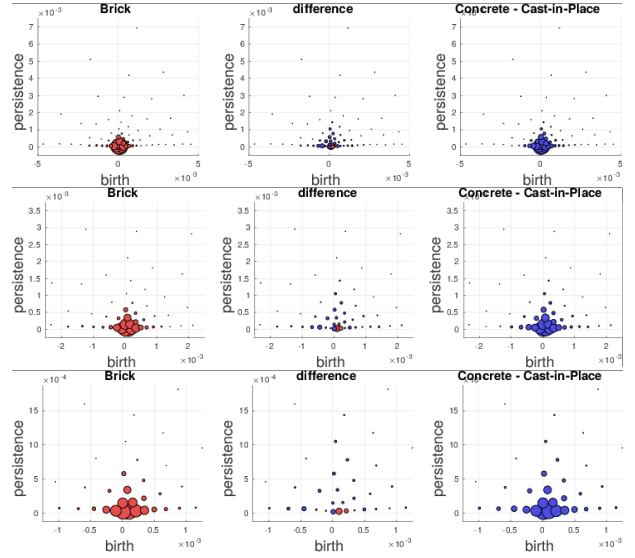


Figure 6: Comparison of averaged PBoW histograms for classes “brick” and “concrete cast-in-place” of the GeoMat dataset (top row: total view, 2nd row: zoomed in view, 3rd row: even further zoomed in view). Left and right PDs show the respective histograms in the birth-persistence plane, while in the center we present difference plots between them. Red color in the difference plot means that the left class has stronger support for this cluster and blue means that the right class has stronger support.

- [2] M. Carrière, M. Cuturi, and S. Oudot. Sliced wasserstein kernel for persistence diagrams. In *ICML*, 2017. 3
- [3] M. Carrière, S. Oudot, and M. Ovsjanikov. Stable topological signatures for points on 3d shapes. In *Computer Graphics Forum*, volume 34, pages 1–12. Wiley Online Library, 2015. 5
- [4] X. Chen, A. Golovinskiy, and T. Funkhouser. A benchmark for 3d mesh segmentation. In *ACM SIGGRAPH 2009 Papers*, SIGGRAPH '09, pages 73:1–73:12, New York, NY, USA, 2009. ACM. 5
- [5] J. DeGol, M. Golparvar-Fard, and D. Hoiem. Geometry-informed material recognition. In *Proceedings of the IEEE Conference on Computer Vision and Pattern Recognition*, pages 1554–1562, 2016. 3, 4
- [6] T. Dey, D. Shi, and Y. Wang. Simba: An efficient tool for approximating rips-filtration persistence via simplicial batch-collapse. In P. Sankowski and C. Zaroliagis, editors, *24th Annual European Symposium on Algorithms, ESA 2016, August 22-24, 2016, Aarhus, Denmark*, volume 57 of *LIPIcs*, pages 35:1–35:16. Schloss Dagstuhl - Leibniz-Zentrum fuer Informatik, 2016. 3
- [7] H. Edelsbrunner and J. Harer. *Computational topology: an introduction*. American Mathematical Soc., 2010. 1, 2, 3
- [8] H. Edelsbrunner, D. Letscher, and A. Zomorodian. Topological persistence and simplification. *Discrete and Computational Geometry*, 28:511–533, 2002. 1
- [9] C. Hofer, R. Kwitt, M. Niethammer, and A. Uhl. Deep learning with topological signatures. In *Advances in Neural Information Processing Systems*, pages 1633–1643, 2017. 3
- [10] M. S. M. Z. C. R. M. S. G. B. A. M. Poier, G. and H. Bischof. Petrosurf3d - a dataset for high-resolution 3d surface segmentation. In *Proceedings of the 15th International Workshop on Content-based Multimedia Indexing (CBMI)*, 2017. 4
- [11] P. Yanardag and S. Vishwanathan. Deep graph kernels. In *Proceedings of the 21th ACM SIGKDD International Conference on Knowledge Discovery and Data Mining*, pages 1365–1374. ACM, 2015. 4
- [12] M. Zeppelzauer, B. Zieliński, M. Juda, and M. Seidl. A study on topological descriptors for the analysis of 3d surface texture. *Computer Vision and Image Understanding*, 2017. 3
- [13] A. Zomorodian and G. Carlsson. Computing persistent homology. *Discrete & Computational Geometry*, 33(2):249–274, 2005. 1